PHYSICAL REVIEW B VOLUME 50, NUMBER 11 15 SEPTEMBER 1994-I

Local structures around Mn luminescent centers in Mn-doped nanocrystals of ZnS

Y. L. Soo, Z. H. Ming, S. W. Huang, and Y. H. Kao
Department of Physics, State University of New York at Buffalo, Buffalo, New York 14260

R. N. Bhargava
Nanocrystals Technology, P.O. Box 820, Briarcliff Manor, New York 10510

D. Gallagher
Philips Laboratories, Philips Electronics North America Corporation, 345 Scarborough Road, Briarcliff Manor, New York 10510

(Received 21 March 1994; revised manuscript received 19 May 1994)

X-ray-absorption fine-structure measurements were carried out to probe the local environment surrounding Mn ions in Mn-doped nanocrystals of ZnS with different size distributions ranging from 30–35 Å to 50–55 Å. The interatomic distances between Mn and neighboring atoms, the coordination number, local disorder, and effective valency determined for the nanocrystals are compared with those in bulk Mn-doped ZnS. The Mn ions are found to substitute for the Zn sites in the host ZnS but with significant size-dependent local structural changes. The questions of Mn-cluster formation and the presence of Mn impurities on the surface of the nanocrystals are addressed. Near-edge x-ray-absorption fine structures indicate that the effective valency of Mn ions in the nanocrystals is close to +2 with a weak size dependence. These local structures are believed to be closely related to the novel optical properties observed in this new class of semiconductors.

INTRODUCTION

Recently, there has been considerable interest in the study of compound semiconductors with dimensions on the nanometer scale. This class of new materials has not only provided many unique opportunities for studying physics in low dimensions but also exhibited novel optical and transport properties which are potentially useful for technological applications. Of special interest is the advent of doped semiconductor nanocrystals (e.g., ZnS:Mn).[1–3] In contrast to the undoped nanocrystals (e.g., ZnS particles)[4] or bulk alloys (e.g., ZnMnS),[5] the impurity states in a doped semiconductor nanocrystal can play a special role in affecting the electronic energy structures and transition probabilities. As a result of confinement effects on the energy states and scattering rates, unusual physical behaviors are expected to emerge in semiconductor nanocrystals when their sizes are reduced to sizes comparable to some characteristic lengths, such as the electronic de Broglie wavelength, effective Bohr radius around the impurity centers, exciton radius, etc. Indeed, high photoluminescent quantum efficiency and greatly enhanced transition rates associated with Mn luminescent centers have recently been observed in Mn-doped ZnS nanocrystals of sizes ranging from 70 to 30 Å.[1–3] The luminescent decay time was found to decrease with the particle size and was at least five orders of magnitude faster than the corresponding Mn^{2+} radiative transition in the bulk crystals.[1]

The drastic changes of optical properties in the doped nanocrystals are clearly related to the nature and local structure of the luminescent center in the material. Consider a 0.5% level of Mn doping in a nanosized ZnS particle with diameter around 30 Å. On average, there is only a single Mn impurity center within such a ZnS host. Because of the small size of the system, this single impurity center could give rise to significant changes in the physical properties as a result of symmetry breaking, crystal-field distortion, size quantization, and hybridization of host *s*-*p* states with *d* states of Mn. The enhanced transition probability, as well as the decay rate of the Mn ion, should therefore be closely related to the local structure around the Mn ions resulting from the ionic size difference and valence mismatch between the dopant and the host cations. It seems highly desirable, therefore, to obtain a clear picture of the local structures around the Mn dopants, such as the location of Mn in the nanocrystal, local distortions in the bond lengths, and the dopant valency. In addition, the possibilities of Mn-cluster formation and the presence of Mn ions near the surface could also significantly influence the luminescence efficiency,[6] so these questions should also be studied.

The present work is aimed at a quantitative determination of the local structures in ZnS:Mn nanocrystals of different size distributions using x-ray-absorption fine structure (XAFS). Because the impurities in these nanocrystals lack long-range structural order, conventional x-ray-diffraction methods are not useful for this purpose. The short-range nature of extended x-ray-absorption fine structure (EXAFS), however, makes this technique uniquely suited for this task.

EXPERIMENTAL

Two ZnS:Mn nanocrystal materials (samples *A* and *B*) with different size distributions, as well as a bulk ZnS:Mn reference sample, were studied in the present XAFS experiments. Samples *A* and *B* contain particles with aver-

0163-1829/94/50(11)/7602(6)/$06.00

age diameters of 50–55 and 30–35 Å, respectively, as determined from transmission electron microscopy measurements. The Mn content in the nanocrystals was found to be ~0.5 at. % using energy-dispersive x-ray spectroscopy. To prepare the nanocrystal ZnS:Mn samples, ZnS was first formed in an exchange reaction of diethylzinc $(C_2H_5)_2Zn$ with solubilized hydrogen sulfide, and then precipitated as a nanocrystal powder in a toluene solvent. Doping of Mn in the nanocrystal ZnS powder was achieved by adding diethylmanganese $(C_2H_5)_2Mn$, which was produced by reacting manganese chloride with ethylmagnesium chloride C_2H_5MgCl. Methacrylic acid surfactant $C_4H_6O_2$ was used to maintain separation of the precipitated particles. In contrast to the nanocrystal powders, the bulk ZnS powders were doped by thermal diffusion of Mn at temperatures > 1100 °C for several hours.

The EXAFS and near-edge x-ray-absorption fine-structure (NEXAFS) measurements were performed at beamline X3B1 at the National Synchrotron Light Source. A Si(111) double-crystal monochromator located 10.8 m from the source and a 0.2 mm vertical slit positioned 75 cm downstream were used for scanning the photon energy. The energy resolution of the incident beam was estimated to be about 0.2 eV at the Mn *K* edge (6539 eV). To minimize the effects of higher harmonics after the monochromator, the second crystal was tilted such that the intensity of the incident beam was detuned to 50% of its maximum at the Mn *K* edge. A nitrogen-flowing ionization chamber was used as the beam monitor. Due to the low Mn concentrations, all three ZnS:Mn samples were measured in the fluorescence mode. An energy-dispersive solid-state Si(Li) detector (energy resolution of 165 eV at the Mn $K\alpha$ fluorescence line) mounted parallel to the electric field of the incident radiation was used. All model compounds from Johnson Matthey Inc. were measured in trasmission using a second nitrogen-flowing ionization chamber. In the NEXAFS measurements, bypassed incident x-rays (in the case of fluorescence detection) or transmitted x rays (in the case of transmission detection) passed through a thin Mn metal foil followed by an additional nitrogen-flowing ionization chamber to provide an energy reference for the upstream measurements. Sample *B* was attached to a 40 K cold finger of a cryostat during the EXAFS measurements. All other data were obtained from room-temperature samples.

DATA ANALYSIS

An improved background removal method[7] was used to extract the EXAFS χ functions from the raw experimental data [Fig. 1(a)]. In accord with standards set at the 1988 international workshop at Brookhaven National Laboratory, several corrections have been taken into account in the data reduction process. For fluorescence data, the energy dependence of the beam monitor was corrected using photoabsorption tables published by Henke *et al.*;[8] self-absorption effects were neglected due to the low Mn concentration in the ZnS:Mn samples. Corrections to the χ functions were made using the McMaster coefficients.[9] The χ functions were then weighted with k^3 and Fourier transformed into real (R) space.[10] Two main peaks are present in the Fourier-transform magnitude functions [Fig. 1(b)] for all three ZnS:Mn samples studied. The first peak at ~2 Å is attributed to the nearest S neighbors, while the second peak at ~3–4 Å is due mainly to more distant Zn and S neighbors. In addition, a weak peak located at ≲3 Å in the data of sample *A* is taken as an indication of possible formation of Mn clusters.

To interpret the results quantitatively, curve fitting in *k* space was performed on the three ZnS:Mn samples. To search for the optimum values of the fitting parameters, we have developed an automatic code based on the down-hill simplex method and χ^2 fitting method.[11] The formula used to calculate the theoretical χ function in our program is[12]

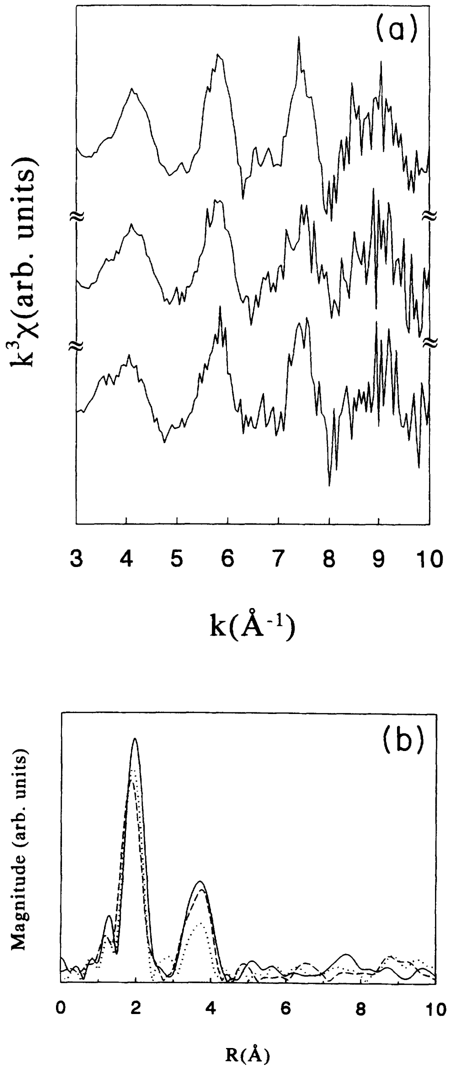

FIG. 1. (a) Weighted EXAFS functions $k^3\chi$ (from top: bulk ZnS:Mn, sample *A*, and sample *B*). (b) Fourier-transform magnitude of the EXAFS functions in (a); bulk ZnS:Mn (solid line), sample *A* (dotted line), and sample *B* (dashed line).

TABLE I. Local structure around Mn in bulk and nanocrystal Mn-doped ZnS samples obtained from curve-fitting the filtered first peak in the Fourier-transformed data. Underline values were kept constant during fitting. Uncertainties were estimated by the double-minimum residue ($2\chi^2$) method.

Sample	$R_{\min}-R_{\max}$ (Å)	Atom	N	R (Å)	σ^2 (10^{-3} Å^2)	ΔE_0 (eV)	S_0^2	$10\chi^2$
Bulk	1.42–2.46	S	4	2.42±0.01	4.1±0.3	2.0±0.3	0.81±0.01	1.27
Sample *A*	1.40–2.44	S	3.6±0.2	2.39±0.01	4.8±0.6	−1.9±0.5	0.81	5.26
Sample *B*	1.28–2.40	S	3.2±0.4	2.36±0.01	4±3	−7±5	0.81	16.7

$$\chi(k)=S_0^2\sum_j \frac{N_j}{kR_j^2}F_j(k)\exp(-2k^2\sigma_j^2)\times\exp\left[\frac{-2(R_j-\Delta)}{\lambda}\right]\sin[2kR_j+\delta_j(k)]\ , \qquad (1)$$

where S_0^2 is the amplitude reduction factor representing the central atom shakeup and shakeoff effects, and λ is the mean free path of photoelectrons. Both S_0^2 and λ were determined by curve fitting the bulk ZnS:Mn model compound whose coordination number is known. $F_j(k)$ and $\delta_j(k)$, the magnitude of the backscattering amplitude of the jth-neighbor shell and the corresponding phase shift due to the atomic potential, respectively, are extracted from theoretical model EXAFS functions calculated by FEFF.[13] Δ can be satisfactorily approximated by the mean distance between the absorbing atom and the first-neighboring shell.[12] Thus the remaining parameters left to be determined are N_j, R_j, σ_j^2, and ΔE_0^j, where N_j is the number of atoms in the jth-neighboring shell, R_j is the mean distance between the absorbing atom and the jth shell, σ_j^2 is the mean-square relative displacement, and ΔE_0^j is the difference between the theoretical and actual zero kinetic energy values. Akima interpolation[14] was employed whenever the values between two tabulated points in the extracted backscattering amplitude and phase-shift files were needed.

During the fitting procedures, our program calculated the theoretical $k^3\chi$ functions at exactly the same k points as those of the experimental $k^3\ \chi$ functions, and then exactly the same Fourier-filtering procedures were imposed. In this way, any distortions of the filtered experimental $k^3\ \chi$ functions due to windowing and approximate mathematical operations were made identical in their calculated counterparts. Such procedures allow more reliable fitting of short-range data.

The local structure around Mn in bulk ZnS:Mn is known from other studies.[15,16] Mn substitutionally occupies the Zn site, which has a nearest-neighbor shell of four S atoms at 2.342 Å and second- and third-neighbor shells of 12 Zn and 12 S atoms at 3.825 and 4.485 Å, respectively. These parameters are used in fitting the Fourier-filtered $k^3\ \chi$ function arising from the first-neighboring shell [i.e., the first peak in Fig. 1(b)]. The window function used in the Fourier-filtering process was composed of a rectangular part in the center and Hanning parts on the sides with a Hanning fraction[12] of 0.2. With the coordination number of the bulk sample being fixed, we obtained S_0^2, which was then used in fitting the nanocrystal samples. Figures 2(a), (b), and (c) illustrate

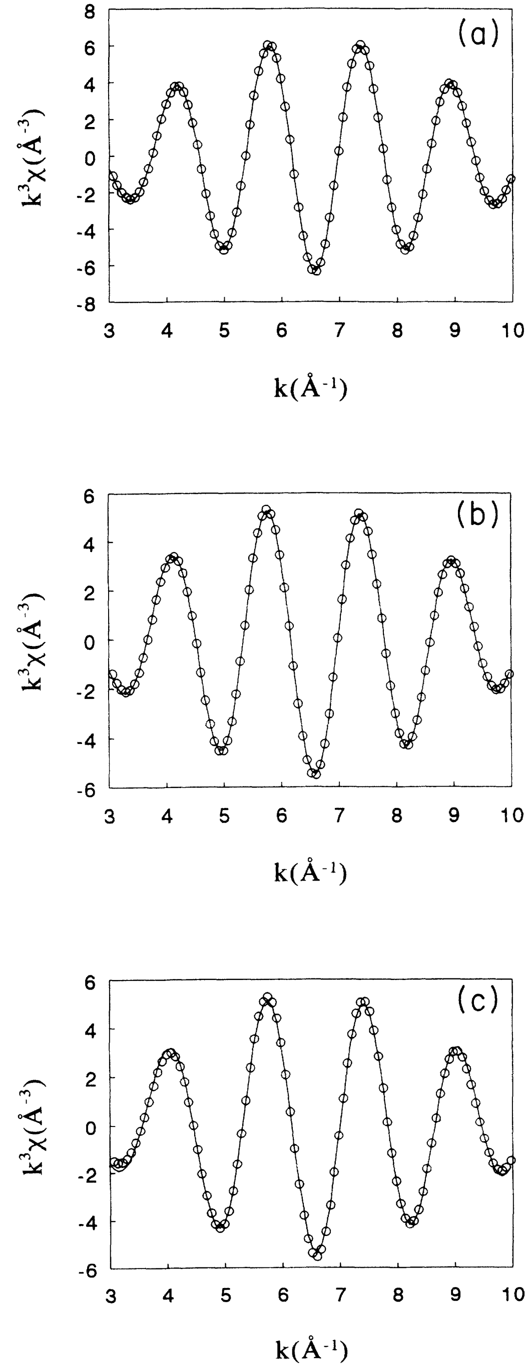

FIG. 2. Least-squares fit of filtered first-shell $k^3\chi$ function for (a) the bulk sample, (b) sample *A*, (c) sample *B*. Circles: data, line: calculation based on parameters given in Table I.

TABLE II. Local structure around Mn in bulk and nanocrystal Mn-doped ZnS samples obtained from curve-fitting the first and second main peaks in the Fourier-transformed data. Underlined values were kept constant and the asterisked value was set as a lower limit during fitting. Uncertainties were estimated by the double-minimum residue ($2\chi^2$) method.

Sample	$R_{\min}-R_{\max}$ (Å)	Atom	N	R (Å)	σ^2 (10^{-3} Å^2)	ΔE_0 (eV)	S_0^2	λ (Å)	$10\chi^2$
Bulk	1.42–2.46	S	4	2.421±0.005	4.4±0.7	2.1±0.7	0.82±0.05	3.2±4	6.94
	2.88–4.44	Zn	12	3.86±0.03	12.4±3	−1±4			
		S	12	4.47±0.04	13.8±30	−1±4			
Sample *A*	1.40–2.44	S	3.6±0.2	2.395±0.005	5.1±0.7	−2.1±0.5	0.82	3.2	6.44
	3.04–4.56	Zn	7±6	3.85±0.03	12.4*	0±5			
		S	7±6	4.32±0.05	19±8	−8±5			
Sample *B*	1.36–2.40	S	3.2±0.4	2.363±0.005	5±3	−7±5	0.82	3.2	17.2
	2.88–4.44	Zn	12±4	3.85±0.03	13±3	−5±5			
		S	15±4	4.36±0.04	13.8*	−7±5			

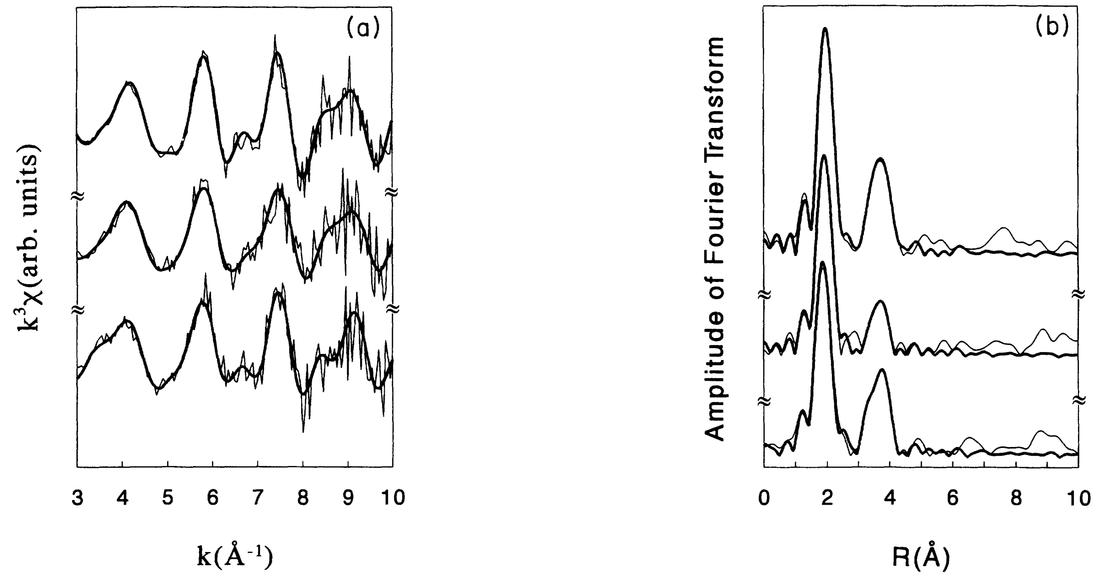

FIG. 3. (a) Experimental $k^3\chi$ (fine lines) compared with the calculated EXAFS function based on parameters for main-peaks fitting listed in Table II ($k^3\chi'$) (coarse lines) (from top: bulk ZnS:Mn, sample *A*, and sample *B*. (b) Magnitude of Fourier transform (FT) of experimental $k^3\chi$ (fine lines) compared with FT of calculated EXAFS function based on parameters of main-peaks fitting listed in Table II ($k^3\chi'$) (coarse lines) (from top: bulk ZnS:Mn, sample *A*, and sample *B*).

TABLE III. Local structure around Mn in sample *A* (Mn-doped ZnS nanocrystal, 50–55 Å) obtained from curve-fitting the first and second main peaks along with an assumed Mn shell in the Fourier-transformed data. Underlined values were kept constant and the asterisked value was set as a lower limit during fitting. Uncertainties were estimated by the double-minimum residue ($2\chi^2$) method.

$R_{\min}-R_{\max}$ (Å)	Atom	N N	R (Å)	σ^2 (10^{-3} Å^2)	ΔE_0 (eV)	S_0^2	λ (Å)	$10\chi^2$
1.36–4.76	S	3.4±0.2	2.393±0.005	4.5±0.6	−2.2±0.5	0.82	3.2	5.37
	Mn	1.3±0.8	2.92±0.03	12±6	13±5			
	Zn	7±3	3.86±0.03	12.4*	1±4			
	S	8±5	4.35±0.04	21±8	−6±5			

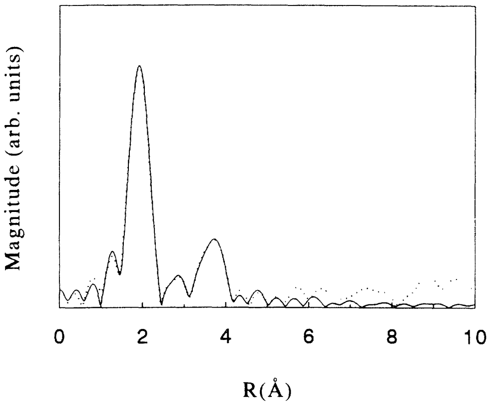

FIG. 4. Fourier-transform magnitude of experimental EXAFS function ($k^3\chi$) (dots) compared with that of calculated total k^3-weighted EXAFS function (including the possible Mn shell, see Table III) (line) for sample *A*.

the final results of the fits, with the corresponding structural parameters listed in Table I.

Structural information of more distant shells was obtained using a three-shell fitting procedure. Similar to the first-shell fitting, the known coordinations in the neighboring shells of the bulk sample were used to obtain the value of S_0^2. For the nanocrystal samples, all four parameters for the first shell were allowed to vary. However, the second peak at ~3–4 Å contains both Zn and S shells (assuming a Zn-site substitution model), so proper constraints on the fitting parameters are required to obtain consistent fitting results. We assumed that the disorder parameter σ^2 in the Zn and S shells in the second main peak for both nanocrystal samples cannot be smaller than those in the bulk sample (0.0124 Å^2 for Zn, 0.0138 Å^2 for the S shell). Curve fitting based on this physically reasonable assumption gives satisfactory results (see Table II). In Fig. 3(a), we have superposed the $k^3\ \chi$ functions calculated with these fitting parameters (heavy solid line) on the experimental data from all three ZnS:Mn samples. The corresponding Fourier-transform magnitude functions are plotted in Fig. 3(b). Finally, a four-shell fit, now including the weak peak at $\lesssim 3$ Å and attributed to Mn, was carried out for sample *A*. The result are listed in Table III, and the Fourier transforms of the so-calculated and experimental data are shown in Fig. 4.

RESULTS AND DISCUSSION

When Mn atoms are added to the host lattice of ZnS, three types of Mn microstructures could, in general, be formed: (i) Mn atoms substitutionally occupying Zn sites, (ii) Mn clusters, and (iii) MnS complexes. These possibilities can be addressed directly by examining the EXAFS data shown in Figs. 1–4.

Consider first the possibility of forming clusters of MnS. In such an environment, the Mn ion is coordinated to six S atoms at a distance of 2.61 Å. The excellent fits to the first-neighbor shell shown in Figs. 2(a)–2(c) and summarized in Table I immediately preclude this structure, because Mn is found to be coordinated to no more than approximately four S atoms at distances no greater than ~2.4 Å.

By contrast, the distances and coordination numbers around Mn in all three samples studied (see Table II) are fully consistent with the Mn atoms occupying Zn sites in ZnS. There is an obvious local distortion around Mn in that the first-neighbor Mn-S distances are always slightly larger than the first-neighbor Zn-S distance of 2.34 Å in bulk ZnS.[16,17] This built-in local distortion could stem from the differences in the ionic size and valency between Mn and Zn in their formation of *covalent* bonds with the S atoms. Qualitatively, our observation of such behavior in all three samples is consistent with the fact that no apparent differences were found in the luminescent spectra of the bulk and nanocrystalline ZnS:Mn.[1–3] Quantitatively, however, we do find a *size-dependent* variation in the local environment around the Mn atoms. The first-neighbor bond length decreases from the bulk value by ~0.02 Å in sample *A* and ~0.05 Å in sample *B*. This bond-length decrease with decreasing nanocrystal size could imply either an enhanced interaction between Mn *d* orbitals and *s-p* electron-hole pairs in ZnS or an increased cross section for electron-hole capture at the impurity site. A size dependence has also been observed[1] in the luminescence efficiency of ZnS:Mn nanocrystals.

Within our experimental uncertainties, the interatomic distance between Mn and second-neighbor Zn atoms seems to remain unchanged as the particle size is reduced from bulk to 30 Å. On the other hand, the interatomic distance between Mn and third-neighbor S atoms is found to decrease by ~0.1 Å from bulk to nanocrystalline sizes. This result, as well as the local distortion in the first-neighbor shell, indicates that the Zn sublattice remains essentially intact despite the variation in the S sublattice. These observations suggest a possible change in crystal field at the Mn site. We also note that with decreasing particle size there is only a small increase in local disorder around the Mn atoms, as measured by σ^2 (see Table I). This high degree of crystallinity even in the nanocrystallites is essential for achieving light emission with high spectral purity.

The coordination numbers of the second (Zn) and third (S) neighboring shells in sample *A* deserve comment. These numbers show a significant decrease from the corresponding bulk values, albeit with large associated fluctuation uncertainties. This could result from either the formation of Mn clusters (see below) or the presence of more Mn impurities near the particle surface. The former could lead to a lowered recombination rate, while the latter could give rise to higher nonradiative transitions. In either case, the luminescence efficiency would be reduced.

Also of interest in sample *A* is the presence of a small peak between the two main peaks in the Fourier transform [see Figs. 1(b) and 3(b)]. Its origin was investigated with a four-shell curve fit giving the results in Fig. 4 and Table III. The inclusion of a Mn-Mn shell in the analysis does not cause any meaningful changes in the results already obtained in Table II (with no Mn clusters). As

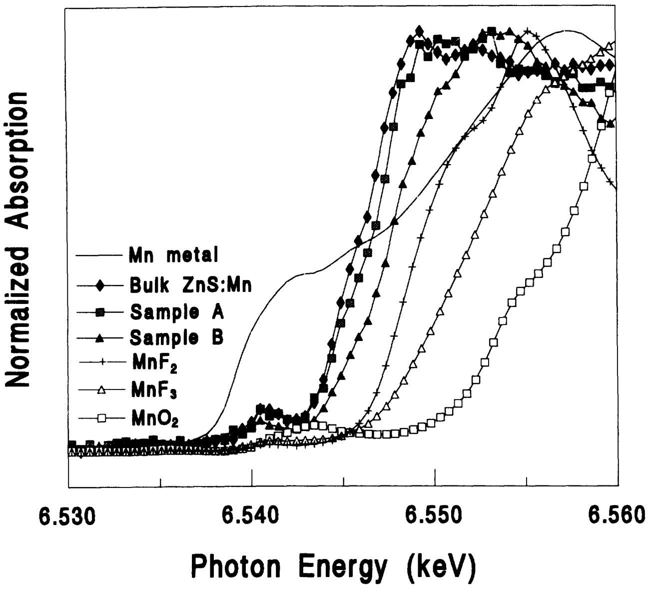

FIG. 5. Normalized absorption of model compounds and samples in the Mn *K* near-edge region.

shown, this small peak is consistent with a microcluster of 2–3 Mn atoms, but is by no means exclusive proof of such a species.

The lowered coordination number around Mn and the possibility of small Mn clusters in sample *A* could also lend some support to the observed size dependence of luminescence efficiency. As reported in Ref. 1, the measured luminescence efficiency was 7% for sample *A* and a higher value of 18% was obtained for sample *B*.

In addition to the EXAFS studies, NEXAFS measurements were made on a series of commercial Mn compounds of known Mn valency, along with a pure Mn sample and the three ZnS:Mn samples investigated. The NEXAFS results are shown in Fig. 5. The threshold occurring at the Mn *K* absorption edge is due mainly to the $1s \rightarrow 4p$ transition. As expected from simple effective-charge arguments, the edge shifts to higher energies as the valency of Mn ions increases from Mn metal (zero valence), to $MnF_2(+2)$, $MnF_3(+3)$, and $MnO_2(+4)$. Using these curves as references, it can be seen that the three ZnS:Mn samples all show an *effective* valency somewhat close to but below +2. There is, however, a *size-dependent* valency increase as the nanocrystal becomes smaller.

CONCLUSION

EXAFS measurements have been carried out to determine the changes in local structure around Mn impurities in ZnS:Mn nanocrystals as the particle size is reduced to values around 30 Å. Interatomic distances, coordination numbers, local disorder, and effective valency around the Mn ions were determined for two nanocrystal samples and compared with corresponding values in bulk ZnS:Mn. Owing to the differences in ionic size and valency between Mn and Zn, significant local structural changes were found which could account for some of the novel optical properties observed in these nanocrystal semiconductors.

ACKNOWLEDGMENTS

The present research at SUNY Buffalo was supported by U.S. Department of Energy under Grant No. DE-FG02-87ER-45283. Research carried out in part at the National Synchrotron Light Source at Brookhaven National Laboratory was supported by the U.S. Department of Energy, Division of Materials Sciences and Division of Chemical Sciences. The SUNY X3 beamline at NSLS is supported by the Division of Basic Energy Sciences of the U.S. Department of Energy (DE-FG02-86ER45231). We also would like to thank J. Racz for the technical support.

---

[1] R. N. Bhargava, D. Gallagher, X. Hong, and A. Nurmikko, Phys. Rev. Lett. **72**, 416 (1994).

[2] R. N. Bhargava, D. Gallagher, and T. Welker, J. Lumin. (to be published).

[3] D. Gallagher, W. Heady, J. Racz, and R. N. Bhargava, J. Cryst. Growth (to be published).

[4] R. Rossetti, R. Hull, J. M. Gibson, and L. E. Brus, J. Chem. Phys. **82**, 552 (1985).

[5] Y. Wang, N. Herron, K. Moller, and T. Bein, Solid State Commun. **77**, 33 (1991).

[6] G. F. Imbusch, in *Luminescence Spectroscopy,* edited by M. D. Lumb (Academic, London, 1978), Chap. 1.

[7] M. Newville, P. Livinš, Y. Yacoby, J. J. Rehr, and E. A. Stern, Phys. Rev. B **47**, 14 126 (1993).

[8] B. L. Henke, P. Lee, T. J. Tanaka, R. L. Shimabukuro, and B. K. Fujikawa, At. Data Nucl. Data Tables **27**, 3 (1982).

[9] W. H. McMaster, N. Kerr Del Grande, J. H. Mallett, and J. H. Hubbell, *Compilation of X-ray Cross Sections* (National Technical Information Services, Springfield, 1969).

[10] P. A. Lee, P. H. Citrin, P. Eisenberger, and B. M. Kincaid, Rev. Mod. Phys. **53**, 760 (1981).

[11] W. H. Press, B. P. Flannery, S. A. Teukolsky, and W. T. Vetterling, *Numerical Recipes* (Cambridge University Press, Cambridge, England, 1986).

[12] D. E. Sayers and B. A. Bunker, in *X-ray Absorption,* edited by D. C. Koningsberger and R. Prins (Wiley, New York, 1988), pp. 211 and 231.

[13] J. J. Rehr, J. Mustre de Leon, S. I. Zabinsky, and R. C. Albers, J. Am. Chem. Soc. **113**, 5135 (1991).

[14] H. Akima, J. Assoc. Comput. Mach. **17**, 589 (1970).

[15] Y. Charreire, D.-R. Svoronos, I. Ascone, O. Tolonen, L. Niinistö, and M. Leskelä, J. Electrochem. Soc. **140**, 2015 (1993).

[16] Ralph W. G. Wyckoff, *Crystal Structures* (Interscience, New York, 1960).

[17] Our Mn-S first-neighbor measurements for Mn-S in ZnS:Mn are also in good agreement with the recent EXAFS results of Ref. 15.